Available online at www.sciencedirect.com
ScienceDirect
Journal of Solid State Chemistry 181 (2008) 480–486
JOURNAL OF SOLID STATE CHEMISTRY
www.elsevier.com/locate/jssc

A facile two-step modifying process for preparation of poly(SStNa)-grafted Fe_3O_4/SiO_2 particles

Zhongli Lei*, Yanli Li, Xiangyu Wei

Key Laboratory of Applied Surface and Colloid Chemistry, Shaanxi Normal University, Ministry of Education, School of Chemistry and Materials Science, Xi'an 710062, PR China

Received 20 August 2007; received in revised form 26 November 2007; accepted 10 December 2007
Available online 1 February 2008

Abstract

This article reports the synthesis of the poly(sodium 4-styrenesulfonate)-grafted Fe_3O_4/SiO_2 particles via two steps. The first step involved magnetite nanoparticles (Fe_3O_4) homogeneously incorporated into silica spheres using the modified Stöber method. Second, the modified silica-coated Fe_3O_4 nanoparticles were covered with the outer shell of anionic polyelectrolyte by surface-initiated atom transfer radical polymerization. The resulted composites were characterized by X-ray diffraction (XRD), transmission electron microscopy (TEM), energy dispersive microscopy (EDS), Fourier transform-infrared (FT-IR), thermogravimetric analysis (TGA), X-ray photoelectron spectroscopy (XPS) and vibration sample magnetometer (VSM). The XRD results indicated that the surface modified Fe_3O_4 nanoparticles did not lead to phase change compared with the pure Fe_3O_4. TEM studies revealed nanoparticles remained monodisperse. The detection of sulfur and sodium signals was a convincing evidence that sodium 4-styrenesulfonate was grafted onto the surface of the magnetic silica in XPS analysis. Finally, super-paramagnetic properties of the composite particles, and the ease of modifying the surfaces may make the composites of important use in mild separation, enzyme immobilization, etc.

Keywords: Poly(SStNa); Fe_3O_4/SiO_2 nanoparticles; Surface-initiated ATRP; Composite particles; X-ray photoelectron spectroscopy

1. Introduction

Nanocomposite materials [1,2] of polymer and magnetic nanoparticles of iron oxides have attracted much interest in recent years because they often encompass the desirable features of both organic and inorganic compounds. These materials consisting of magnetic nano- or microparticles of iron oxides have wide application in biomedical and diagnostic fields, including separation of biochemical products [3], gene manipulation and immunoassay [4], enzyme immobilization [5], magnetic resonance imaging (MRI) contrast agents [6], and magnetically guided site-specific drug delivery agents [7]. Several magnetic particles and magnetic supports, such as microspheres of various biomaterials and bioactive agents encapsulating magnetic particles and copolymer with magnetic particles, have been used with good results [8]. However, due to size constraints, these microparticles cannot be used at a specific location that is relevant to a cellular biochemical process and recently developed microfluidic devices [9–11]. Furthermore, pure magnetic particles are likely to form a large aggregation, alter magnetic properties, and can undergo rapid biodegradation when they are directly exposed to the biological system. Therefore, a suitable coating is essential to prevent such limitations from occurring.

It has been demonstrated that the formation of a passive coating of inert materials such as silica on the surfaces of iron oxide nanoparticles could help prevent their aggregation in liquid and improve their chemical stability [12]. Moreover, polyelectrolyte brushes attached to the surface of silica particles can enhance their stability against flocculation in aqueous media due to the additional steric/electrostatic repulsive forces. Thus, a cationic polyelectrolyte natural macromolecule, such as chitosan, can be

*Corresponding author. Postal address: College of Chemistry and Materials Science, Shaanxi Normal University, Xi'an 710062, PR China. Fax: +86 29 85307774.
E-mail address: zhllei@snnu.edu.cn (Z. Lei).

0022-4596/$ - see front matter © 2007 Elsevier Inc. All rights reserved.
doi:10.1016/j.jssc.2007.12.004

adsorbed onto the anionic polyelectrolyte brush immobilized on the surface of silica to fabricate a dual-layer polyelectrolyte nanoparticle support for enzyme immobilization [13].

Strong polyelectrolytes such as poly(sodium 4-styrenesulfonate) and also polyelectrolyte-based micelles have been extensively investigated [14–21]. Several research groups have reported the preparation and characterization of polyelectrolytes attached to planar or spherical surfaces [22–28]. Some theoretical studies have also been carried out [29,30]. However, polyelectrolytes grafted to surfaces of the magnetic silica nanoparticles have not received much attention.

Among the various methods for polymer attachment, surface-initiated atom transfer radical polymerization (ATRP) has become an important tool for further development of the chemical and physical properties of nanostructures, because it provides an effective method to covalently attach polymer chains in a well-controlled fashion, by which excellent controllability over the molecular weight and polydispersity of graft polymers are obtained [31,32].

Guided by these considerations, we designed a feasible two-step process for preparation of the super-paramagnetic poly(SStNa)-grafted Fe_3O_4/SiO_2 composite particles. First, Fe_3O_4/SiO_2 nanoparticles of core–shell structure were prepared through the modified Stöber method, and successively poly(SStNa)-grafted Fe_3O_4/SiO_2 particles were obtained by ATRP of sodium 4-styrenesulfonate (SStNa) using modified magnetic silica as initiator. The ionic monomer examined in this study was in water/methanol mixtures at ambient temperature. It is anticipated that the polymer–inorganic composite particles may be used as novel separation, immobilization, and absorption materials [33–35]. This paper reports the preparation and characterization of the materials.

2. Experimental section

2.1. Materials

$FeCl_3 \cdot 6H_2O$ and $FeCl_2 \cdot 4H_2O$ were purchased from Fluka. tetraethoxysilane (TEOS), citric acid (99.5%), and aqueous ammonia solution (25 wt%) were analytical grade and commercially available products. 2-Bromopropionyl bromide (BPB, Technical Grade) from Technology of Hongchen Xinxiang He'nan, China, 3-aminopropyltriethoxysilane (APTES, 99.0%, Aldrich) was used as received. Triethylamine (TEA) (Shanghai Chemical Co., China) was refluxed with *p*-toluenesulfhonyl chloride and distilled. The resulting pure TEA was stored over CaH_2. It was refluxed and distilled again before use. 2,2′-bipyridine (bpy) (A.R., 97.0%) provided by Beijing Chemical Co. was recrystallized twice from acetone. CuBr was purified according to a published procedure [36]. SStNa was supplied by Fluka 99% (New York, USA). Ultrapure water (resistivity = 18.2 MX, pH 6.82) was used in all experiments. Other reagents and organic solvents for the initiator synthesis and polymerization were purchased from commercial sources and used without further purification.

2.2. Preparation of magnetite nanoparticles

An iron oxide dispersion was prepared using the method already described [37], based on the coprecipitation of $FeCl_2$ and $FeCl_3$ by adding a concentrated solution of base (25 wt% $NH_3 \cdot H_2O$) into the mixture of iron salts with a molar ratio ($FeCl_2$:$FeCl_3$) of 1:2. The reaction mixture was heated at 80 °C for 30 min, and the medium pH was maintained at 10 by addition of aqueous ammonia solution during the reaction. The magnetite dispersion was then stirred for 1.5 h at 90 °C upon addition of a citric acid solution (0.1 M). N_2 was bubbled throughout the reaction. Subsequently, deionized water was added to wash and redisperse ultrafine magnetic particles. Then, the resultant dispersion was treated by dialysis and adjusted to 2.0 wt%. The obtained magnetite dispersion was defined as magnetic fluid (MF).

2.3. Synthesis of Fe_3O_4/SiO_2 core–shell nanoparticles

Followed Stöber process [38] with some modifications, coating magnetite nanoparticles with silica was carried out in basic alcohol/water mixture at room temperature by using MF as seed. A suspension of the synthesized magnetic nanoparticles (1.00 g) was diluted by a mixture of ethanol (80 mL) and water (16 mL). After addition of ammonia solution (2 mL, 25 wt%), the precursor of TEOS (1 mL) was added to the reaction solution with mechanical stirring at 25 °C for 12 h. The preformed particles were washed to eliminate excess reactants by centrifugation and dried in a vacuum oven at 70 °C.

Fe_3O_4/SiO_2 core–shell nanoparticles in the range of 70 nm were washed with the 'piranha' solution (a mixture of 70 vol% concentrated sulfuric acid and 30 vol% hydrogen peroxide) to remove organic residues and uncoated magnetite nanoparticles. The particles were rinsed with copious amount of deionized water, dried in nitrogen flow.

2.4. Synthesis of polyelectrolyte-grafted Fe_3O_4/SiO_2 nanoparticles

2.4.1. Immobilization of the initiator on the Fe_3O_4/SiO_2 nanoparticles surface

The procedure of immobilization of the surface initiators was shown in Scheme 1. First, the aminated Fe_3O_4/SiO_2 nanoparticles were synthesized by reaction with APTES in toluene under nitrogen for 4 h at 95 °C. After the reaction, the nanoparticles were filtered and washed with methanol. Then, the Fe_3O_4/SiO_2 nanoparticles were washed carefully with toluene and finally dried in vacuum oven for the latter step. Second, the above-modified magnetic silica nanoparticles were dispersed in a solution of TEA (2 mL) and freshly distilled toluene (10 mL) under magnetic stirring.

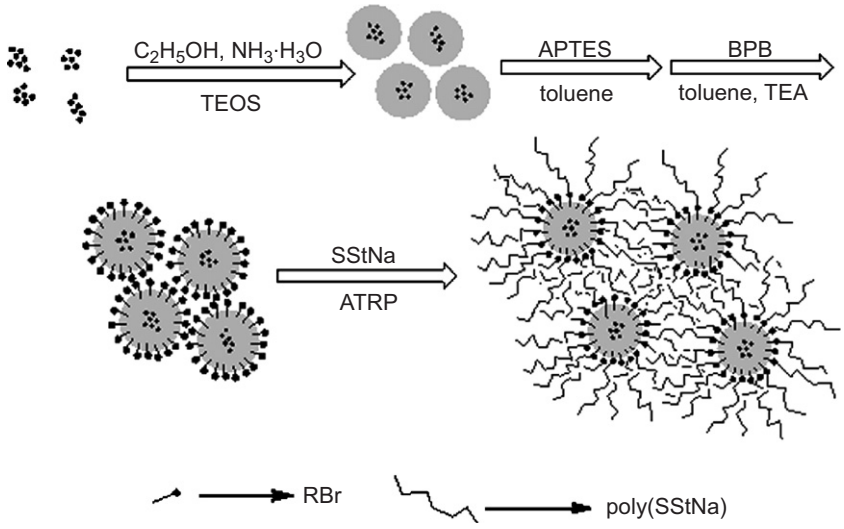

Scheme 1. Schematic representative for preparation of the poly (SStNa)-grafted Fe_3O_4/SiO_2 particles.

After the above mixture was cooled down to 0 °C, a solution of BPB (2 mL) and toluene (5 mL) was added drop wise. After 4 h, the magnetic silica nanoparticles were washed again with toluene and acetone thoroughly, and then dried under vacuum for the subsequent polymerization.

2.4.2. ATRP of sodium 4-styrenesulfonate

The initiator-grafted Fe_3O_4/SiO_2 nanoparticles were then used for the ATRP of SStNa ionic monomers under various reaction conditions. In a typical protocol, the surface-modified Fe_3O_4/SiO_2 nanoparticles (0.30 g) were dispersed in 6.0 mL of a 3:1 (v/v) water/methanol mixture with the aid of an ultrasonic bath. SStNa (539.0 mg) and 2,2′-bipyridine (bpy, 41.1 mg) were then added to this magnetic colloidal dispersion. The mixture was degassed using a nitrogen purge for 30 min with continuous stirring at room temperature. Copper (I) bromide (CuBr, 19.2 mg) was then added under nitrogen. After 3 h, the polymerization was terminated by exposure to air. The reaction mixture was centrifuged at 8000 rpm for 10 min. The supernatant was removed and replaced with doubly distilled, deionized water and the blue ATRP catalyst-contaminated sediment was redispersed in this medium with the aid of an ultrasonic bath. This centrifugation–dispersion cycle was repeated three times to obtain brown, purified polyelectrolyte-grafted Fe_3O_4/SiO_2 nanoparticles.

2.5. Characterization and instrumentation

The sample was characterized by X-ray diffraction (XRD), and XRD scans were obtained using a Rigaku model D/max2000PC X-ray diffractometer operating with a Cu anode at 40 kV and 50 mA in the range of 2θ value between 10° and 80° with a speed of 2 min^{-1}. Transmission electron microscopy (TEM) observation was performed on a Philips H-600 EX TEM operated at a 120 kV accelerating voltage. Specimens for solutions TEM were prepared by spreading a small drop of the sample onto a 400 mesh copper grid and the drop was dried almost completely in air at room temperature for nearly 4 days. Magnetic properties of the samples were measured using a vibration sample magnetometer (VSM, Lake Shore Model 7400) under magnetic fields up to 10 kOe. The saturation magnetization (M_s) was calibrated by a standard bulky nickel rod before the measurement of M_s. Fourier transform-infrared (FT-IR) spectra were recorded in a transmission mode with EQUINX55. The powder samples were ground with KBr and compressed into a pellet. The TGA curves were taken by using a thermogravimetric analyzer from TA Instrument (model Q1000DSC + LNCS + FACS Q600SDT) under a stable N_2 flow. The temperature studied ranged from 20 to 800 °C at a rate of 20 °C/min^{-1}. The surface chemical compositions of the polyelectrolyte-grafted Fe_3O_4/SiO_2 particles were analyzed using X-ray photoelectron spectroscopy (XPS). The XPS spectra were obtained with a Sigma Probe X-ray photoelectron spectrometer (ThermoVG Scientific). The X-ray source was twin anode Al $K\alpha$ radiation (1486.6 eV) and the spot size was 800 μm. Pass energies of 50 eV (for the survey spectra) and 20 eV (for the high-resolution spectra of all the elements of interest) were chosen. C1*s*, N1*s*, O1*s*, Si2*p*, Fe2*p*, S2*p*, and Na1*s* spectra were detected. The sample preparation procedure was as follows. A piece of aluminum foil (0.8 cm × 0.8 cm) was covered with double-sided adhesive tape. The sample powder was then added to mask the entire surface of the tape, and the excess powder was removed to avoid contaminating the XPS spectrometer.

3. Results and discussion

Fig. 1 shows the XRD patterns for pure Fe_3O_4 and silica-coated magnetite nanoparticles. The positions and relative intensities of the reflection peak of Fe_3O_4 nanoparticles agree well with those XRD patterns of Fe_3O_4 nanoparticles in the literature [39–44], which

confirm the structure of the magnetite materials (JCPDS card no.79-0418), indicating the highly crystalline cubic spinel structure. The characteristic peaks at $2\theta = 30.1^\circ$, 35.5°, 43.1°, 53.4°, 57.0° and 62.6° for pure Fe_3O_4 nanoparticles (Fig. 1a), which were marked respectively by their indices (220), (311), (400), (422), (511), and (440), were also observed for Fe_3O_4/SiO_2 nanoparticles (Fig. 1b). This revealed that the surface modified Fe_3O_4 nanoparticles did not lead to their phase change. While the broad peaks at $2\theta = 23$–27° in Fig. 1b were ascribed to amorphous silica, the rest of the peaks of the diffractograms obtained were identified as corresponding to the magnetite (Fe_3O_4) core.

Fig. 2a is TEM image and electron diffraction pattern of the synthesized magnetite nanoparticles, which shows that most of the particles are quasi-spherical with an average diameter of 5–10 nm. Fig. 2b shows TEM images of silica-coated Fe_3O_4 particles. The magnetic silica particles (MSPs) with well-defined core/shell structures were rather monodisperse, even though silica shells had trapped more than one magnetic core. The Fe_3O_4/SiO_2 particles used in this case for the production of composite particles had an average diameter of 70 ± 10 nm obtained by TEM images. The principal idea of the formation of the outer silica shell is to avoid the corrosion of Fe_3O_4 particles. Meanwhile, this was clearly shown for samples with an outer silica shell that kept a stable dispersion compared to those without any protection. As shown in Fig. 2c, a basically core–shell structure (dark colored core for Fe_3O_4/SiO_2 nanoparticles and light-colored shell for poly(SStNa)) was obtained. The samples still remained monodisperse, and total average increase in diameter was approximately 20 nm.

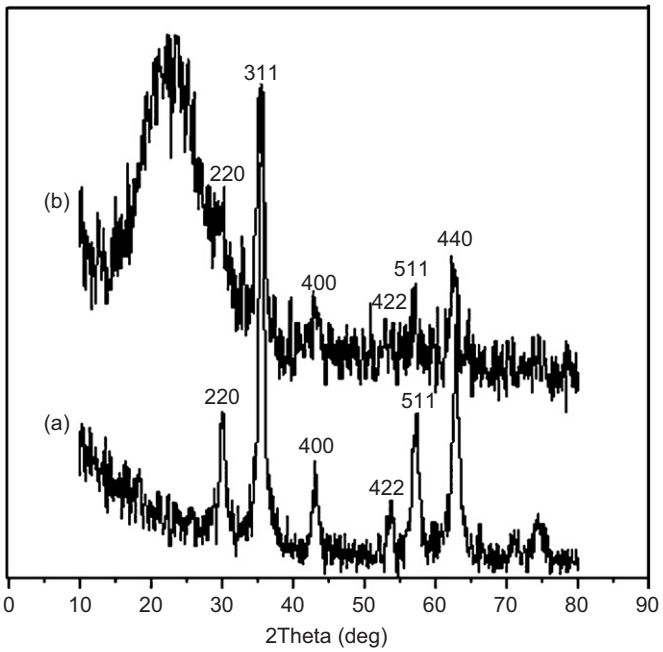

Fig. 1. XRD patterns for (a) pure Fe_3O_4 nanoparticles and (b) silica-coated magnetite particles.

The components of the resulted Fe_3O_4/SiO_2, initiator-functionalized Fe_3O_4/SiO_2 nanoparticles were assayed by energy dispersive X-ray spectrometry (EDS) and elemental mapping analysis. The presence of Si, O, and Fe in Fig. 3a indicated that the iron oxide particles were loaded into silica spheres. The relatively high Si and O peaks could indicate the presence of multiple layers of SiO_2 on the surface of the Fe_3O_4 nanoparticles. The obvious characteristic peak for Br element, originating from modified Fe_3O_4/SiO_2 (Fig. 3b) indicates that the initiators for ATRP are immobilized on the surface of Fe_3O_4/SiO_2 nanoparticles.

Fig. 4 gave the FT-IR spectra of the prepared particles. The analysis indicated absorption centered at 590 cm^{-1} corresponding to the Fe–O vibration related to the magnetite phase. The presence of additional peaks centered at 476, 808, 950, 1110, and 1225 cm^{-1} were most probably due to the symmetric and asymmetric stretching vibration of framework and terminal Si–O– groups. Furthermore, two peaks at 2966 and 2880 cm^{-1} corresponding to C–H stretching absorptions in Fig. 4c can be assigned to poly(SStNa). However, for poly(SStNa)-grafted Fe_3O_4/SiO_2 particles the identification of bands attributable to sulfonate groups (normally a strong IR absorber at 1050 cm^{-1}) was problematic due to overlapping Si–O bands. The peak of the polyelectrolyte-grafted Fe_3O_4/SiO_2 particles was wider and stronger at about 3448.6 cm^{-1},

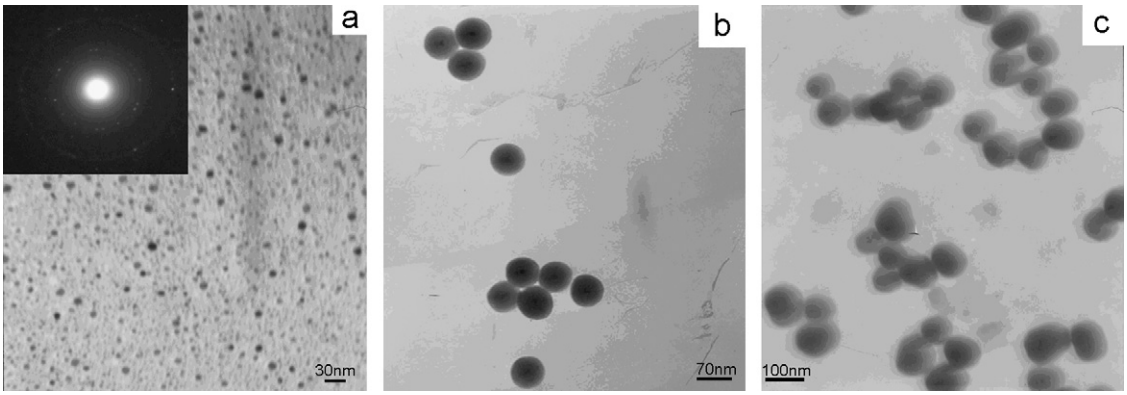

Fig. 2. Transmission electron microscopy (TEM) micrographs of (a) Fe_3O_4 nanoparticles and their electron diffraction pattern, (b) Fe_3O_4/SiO_2 core–shell nanoparticles, (c) poly(SStNa)-grafted Fe_3O_4/SiO_2 particles.

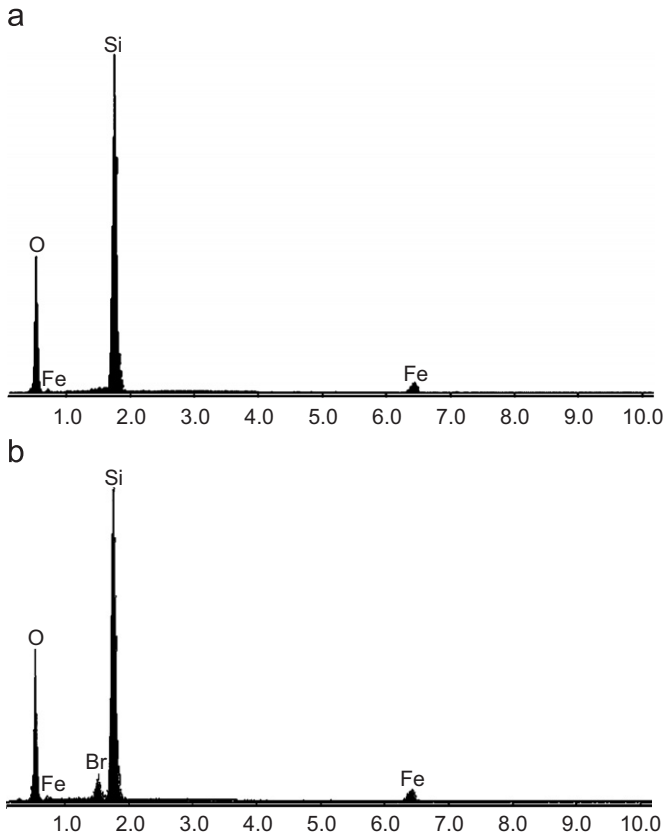

Fig. 3. Energy dispersive X-ray spectrometry (EDS) analysis of (a) silica-coated magnetite particles and (b) initiator-functionalized magnetic silica nanoparticles.

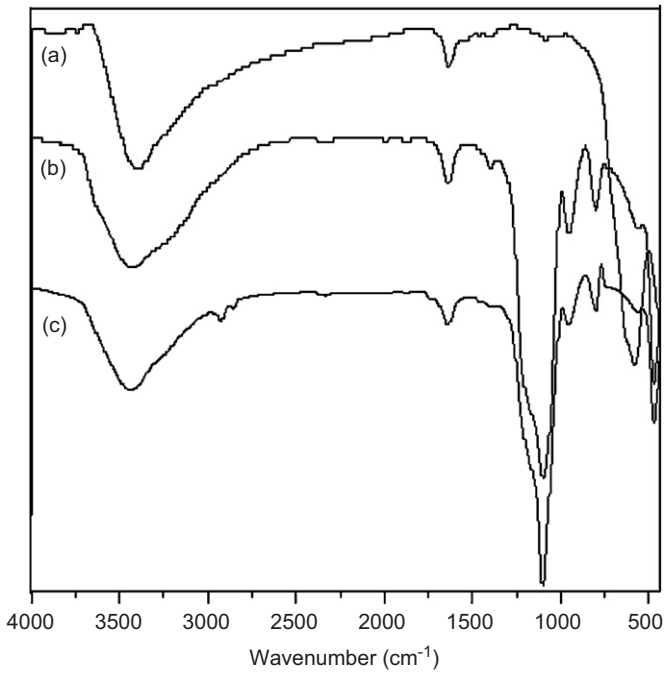

Fig. 4. FT-IR spectra of (a) Fe_3O_4 nanoparticles (b) Fe_3O_4/SiO_2 core–shell nanoparticles, (c) poly(SStNa)-grafted Fe_3O_4/SiO_2 particles.

demonstrating that it carried some free Si–OH permitted by the incompleteness of tetraethoxysilane (TEOS) hydrolysis. Overall, these FT-IR spectra provided supportive evidence that poly(SStNa) polymer chains were successfully grafted onto the Fe_3O_4/SiO_2 nanoparticles surface.

Typical TGA curve for the poly(SStNa)-grafted Fe_3O_4/SiO_2 particles was depicted in Fig. 5. The weight loss below 250 °C was resulted from the release of both the physisorbed and chemisorbed water on the surface of the polymer shell. And the breakout of the structured water occurred above 600 °C. The organic compounds of composite particles were decomposed in the temperature range of 250–600 °C. The weight loss after 250 °C on the TGA curve may also be due to the loss of structure water within amorphous SiO_2. The polymer contents of the composite particles were estimated from the percentage of weight loss from the TGA curve. The weight loss which originated from grafted poly(SStNa) on the Fe_3O_4/SiO_2 particles surface was about 11.56%.

Fig. 6 shows the survey spectra for the polyelectrolyte-grafted Fe_3O_4/SiO_2 particles. The characteristic peaks for C1*s*, O1*s*, Si2*p*, Fe2*p*, Na1*s*, and S2*p* were observed in the spectrum at 285, 533, 104, 701.1, 1071.5, and 167.8 eV respectively. In addition, weak signal at 399.2 eV, corresponding to N1*s*, was also detected. Integration of the peak areas of the elements of interest allowed the surface chemical composition to be calculated for each sample (see Table 1). As expected, poly(SStNa)-grafted Fe_3O_4/SiO_2 particles showed the highest carbon signals, suggesting that the underlying magnetic silica substrates are partially masked by the coated polymer chains. The detection of sulfur and sodium signals is convincing evidence for the presence of poly(SStNa). A relatively weak nitrogen signal was detected for the anionic polyelectrolyte-grafted Fe_3O_4/SiO_2 particles, which is probably due to bipyridine ligand impurities.

The magnetic properties of the composite particles were studied by a vibrating-sample magnetometer. The

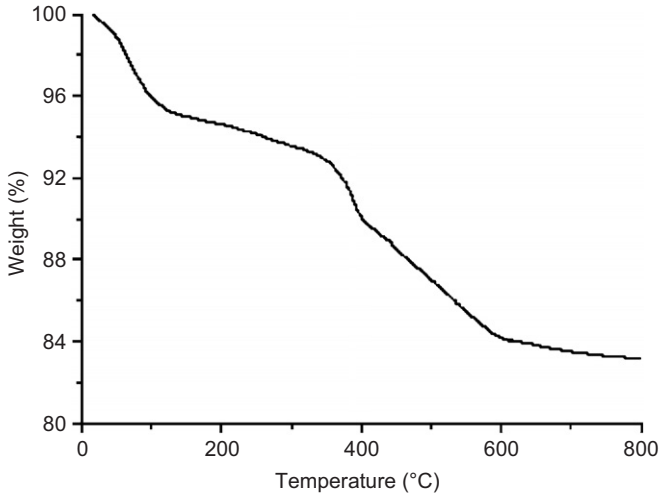

Fig. 5. TGA curves of poly(SStNa)-grafted Fe_3O_4/SiO_2 particles.

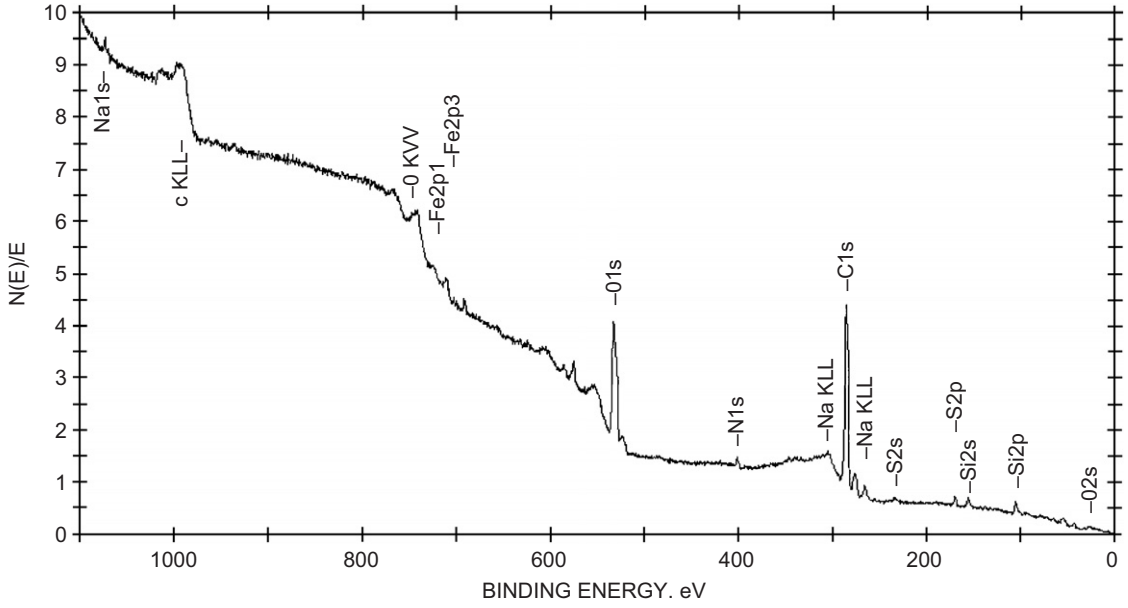

Fig. 6. The survey XPS spectra of poly(SStNa)-grafted Fe_3O_4/SiO_2 particles.

Table 1
XPS surface compositions of the poly(SstNa)-grafted Fe_3O_4/SiO_2 particles

Sample type	Element surface compositions determined by XPS (at %)						
	C1*s*	O1*s*	N1*s*	Si2*p*	Fe2*p*	Na1*s*	S2*p*
Poly(SStNa)-grafted Fe_3O_4/SiO_2	68.54	22.31	1.40	2.61	1.36	1.56	2.23

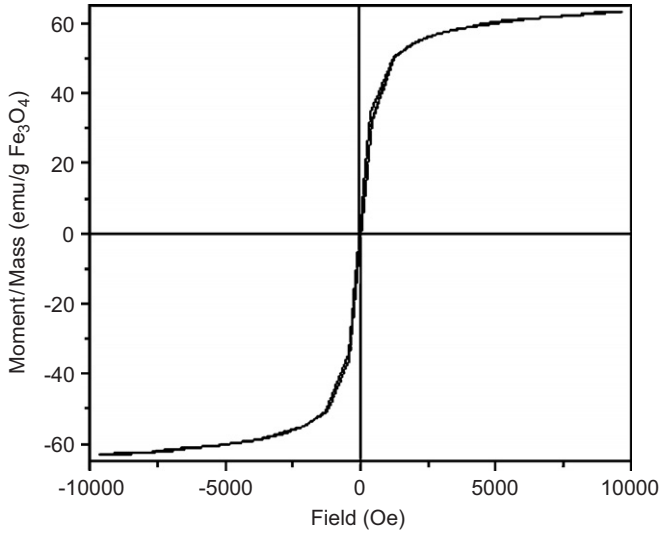

Fig. 7. Magnetic hysteresis loop of as-synthesized Fe_3O_4 nanoparticles.

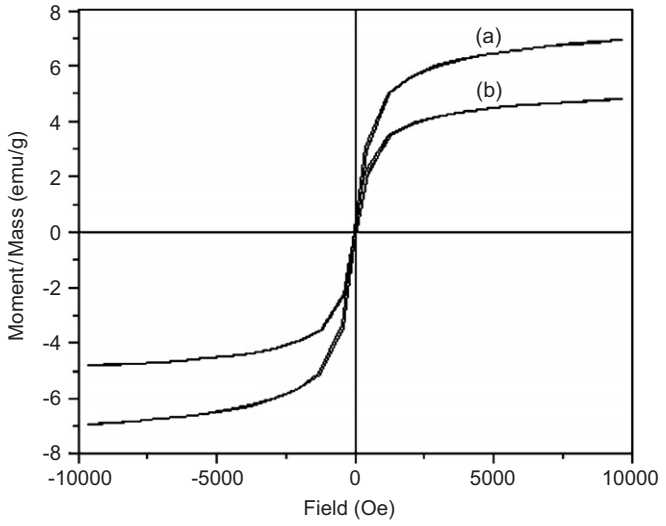

Fig. 8. Magnetization curve of (a) silica-coated magnetite nanoparticles and (b) poly(SStNa)-grafted Fe_3O_4/SiO_2 particles.

saturation magnetization (M_s) of magnetite (in Fig. 7) reduced to 63.292 emu/g of the bulk Fe_3O_4 (92 emu/g of magnetite) [45]. It is known that the energy of a magnetic particle in an external field is proportional to its size via the number of magnetic molecules in a single-magnetic domain. This phenomenon is more significant for the nanoparticles due to their large surface to volume ratio. Therefore, the smaller saturation magnetization value for the nanoparticles compared to the bulk material is reasonable.

As shown in Fig. 8, the saturation magnetic moments of silica-coated Fe_3O_4 particles (Fig. 8a) and polyelectrolyte-grafted Fe_3O_4/SiO_2 particles (Fig. 8b) reached 6.9339 and 4.8154 emu/g, respectively. These low saturation magnetization values were less than the reference value for the pure magnetite nanoparticles (Fe_3O_4). This can be explained by considering the diamagnetic contribution of the silica shells surrounding the magnetite nanoparticles, which also weakened the magnetic moment for poly(SStNa)-grafted Fe_3O_4/SiO_2 particles due to the presence of polymer shells. In addition, both of them showed super-paramagnetic behaviors, indicating that magnetite nanoparticles were still incorporated in the composite particles, which exhibited no remanence effect from the hysteresis loops at applied magnetic field. When the composite particles undergo strong magnetization, the efficient magnetic separation is allowed for, and when the applied magnetic field is removed, redispersion of these particles will take place rapidly. These magnetic properties are critical in the application of the biomedical and bioengineering fields.

4. Conclusions

In summary, we have demonstrated a simple two-step modifying process for preparation of poly(SStNa)-grafted MSPs by functionalizing the surface of magnetic silica particles with an ATRP initiator, followed by surface-initiated polymerization of strong electrolytic monomer in protic media. Successful grafting was confirmed in each case by FT-IR, TGA and XPS. The anionic polyelectrolyte-grafted magnetic silica composite particles show super-paramagnetic properties and occupy basically core–shell structure in the tens of nanometer size range. Considering the super-paramagnetic properties and the ease in chemical modification, these composite particles may find some uses in mild separation, enzyme immobilization, radiation absorption, etc.

References

[1] B.M. Novak, Adv. Mater. 5 (1993) 422.
[2] J. Wen, G.L. Wilkes, Chem. Mater. 8 (1996) 1667.
[3] J. Ugelstad, A. Berge, T. Ellingsen, R. Schmid, T.N. Nilsen, P.C. Mork, P. Stenstad, E. Hornes, O. Olsvik, Prog. Polym. Sci. 17 (1992) 87.
[4] H. Nakayama, A. Arakaki, K. Maruyama, H. Takeyama, Biotechnol. Bioeng. 84 (2003) 96.
[5] H.F. Jia, G.Y. Zhu, P. Wang, Biotechnol. Bioeng. 84 (2003) 406.
[6] C. Billotey, C. Wilhelm, M. Devaud, J.C. Bacri, J. Bittoun, F. Gazeau, Magn. Reson. Med. 49 (2003) 646.
[7] G.V. Patil, Drug. Dev. Res. 58 (2003) 219.
[8] G.Z. Wang, Y. Zhang, Y. Fang, J. Am. Ceram. Soc. 90 (2007) 2067.
[9] D.R. Reyes, D. Iossifidis, P.A. Auroux, Anal. Chem. 74 (2002) 2623.
[10] S.R. Quake, A. Scherer, Science 290 (2000) 1536.
[11] W. Zhan, J. Alvarez, L. Sun, R.M. Crooks, Anal. Chem. 74 (2002) 1233.
[12] See, for example, (a) M.D. Butterworth, L. Illum, S.S. Davis, Colloids Surf. A 179 (2001) 93. (b) D.V. Szabo, D. Vollath, AdV. Mater. 11 (1999) 1313. (c) L.N. Donselaar, A.P. Philipse, J. Suurmond, Langmuir 13 (1997) 6018.
[13] Z.L. Lei, S.X. Bi, H. Yang, Food Chem. 104 (2007) 577.
[14] (a) Z. Tuzar, K. Procházka, I. Zuzková, P. Munk, ACS Polym. Prepr. 34 (1) (1993) 1038;
(b) M. Sedlák, ACS Polym. Prepr. 34 (1) (1993) 1044;
(c) H. Matsuoka, D. Schwahn, N. Ise, ACS Polym. Prepr. 34 (1) (1993) 1046;
(d) W. Essafi, F. Lafuma, C.E. Williams, ACS Polym. Prepr. 34 (1) (1993) 1048;
(e) W.F. Reed, ACS Polym. Prepr. 34 (1) (1993) 1040;
(f) E.J. Amis, M. Sedlak, ACS Polym. Prepr. 34 (1) (1993) 1042.
[15] H. Matsuoka, D. Schwahn, N. Ise, Macromolecules 24 (1991) 4227.
[16] M. Drifford, J.P. Dalbiez, J. Phys. Chem. 88 (1984) 5368.
[17] (a) R.S. Koene, M. Mandel, Macromolecules 16 (1983) 220;
(b) R.S. Koene, T. Nicolai, M. Mandel, Macromolecules 16 (1983) 227.
[18] L.I. Gabaston, S.A. Furlong, R.A. Jackson, S.P. Armes, Polymer 40 (1999) 4505.
[19] D.A. Styrkas, V. Bütün, J.R. Lu, Langmuir 16 (2000) 5980.
[20] (a) V. Bütün, A.B. Lowe, N.C. Billingham, S.P. Armes, J. Am. Chem. Soc. 121 (1999) 4288;
(b) E.J. Lobb, I.Y. Ma, N.C. Billingham, S.P. Armes, J. Am. Chem. Soc. 32 (2001) 7913.
[21] A. Bhattacharyya, F. Monroy, D. Langevin, Langmuir 16 (2000) 8727.
[22] F. Caruso, H. Lichtenfeld, H. Mohwald, M. Giersig, J. Am. Chem. Soc. 120 (1998) 8523.
[23] (a) C. Biver, R. Hariharan, J. Mays, W.B. Russel, Macromolecules 30 (1997) 1787;
(b) R. Hariharan, C. Biver, J. Mays, W.B. Russel, Macromolecules 31 (1998) 7506.
[24] X. Guo, M. Ballauff, Langmuir 16 (2000) 8719.
[25] X. Guo, A. Weiss, M. Ballauff, Macromolecules 32 (1999) 6043.
[26] Y. Shi, C. Seliskar, J. Chem. Mater. 9 (1997) 821.
[27] H. Mori, D. Chan Seng, M. Zhang, A.H.E. Müller, Langmuir 18 (2002) 3682.
[28] D.E. Bergbreiter, K. Sirkar, R.J. Russell, M.V. Pishko, Anal. Chem. 71 (1999) 3133.
[29] P. Pincus, Macromolecules 24 (1991) 2912.
[30] R. Hariharan, C. Biver, W.B. Russel, Macromolecules 31 (1998) 7514.
[31] S.G. Boyes, B. Akgun, W.J. Brittain, Macromolecules 36 (2003) 9539.
[32] X.W. Fan, L.J. Lin, P.B. Messersmith, Composites Sci. Technol. 66 (2006) 1198.
[33] S. Santra, R.P. Bagwe, D. Dutta, Adv. Mater. 17 (2005) 2165.
[34] G. Xie, Q. Zhang, Z. Luo, J. Appl. Polym. Sci. 87 (2003) 1733.
[35] H. Ai, C. Flask, B. Weinberg, X. Shuai, Adv. Mater. 17 (2005) 1949.
[36] R.N. Keller, H.D. Wycoff, Copper (I) Chloride, Inorg. Synth. 2 (1947) 1–4.
[37] F. Sauzedde, A. Elaïssari, C. Pichot, Colloid Polym. Sci. 277 (1999) 846.
[38] W. Stöber, A. Fink, E. Bohn, J. Colloid Interface Sci. 26 (1968) 62.
[39] R. Maoz, E. Frydman, S.R. Cohen, AdV. Mater. 12 (2000) 424.
[40] F. Stephen, R. Hakan, R.S. Nagaraja, Chem. Mater. 14 (2002) 3643.
[41] S.H. Sun, H. Zeng, D.B. Robinson, J. Am. Chem. Soc. 126 (2004) 273.
[42] T.Y. Kim, M.S. Lee, Y.I. Kim, J. Phys. D: Appl. Phys. 36 (2003) 1451.
[43] L.A. Harris, J.D. Goff, A.Y. Carmichael, Chem. Mater. 15 (2003) 1367.
[44] T.Z. Yang, C.M. Shen, H.J. Gao, J. Phys. Chem. B 109 (2005) 23233.
[45] V.S. Zaitsev, D.S. Filimonov, I.A. Presnyakov, J. Colloid Interface Sci. 212 (1999) 49.